energies

MDPI

Article

Water Chemistry Impact on Activated Corrosion Products: An Assessment on Tokamak Reactors

Martina Molinari [1,*], Matteo D'Onorio [1], Giovanni Mariano [2], Nicholas Terranova [2] and Gianfranco Caruso [1,*]

[1] Department of Astronautical, Electrical and Energy Engineering (DIAEE)—Nuclear Section, Sapienza University of Rome, Corso Vittorio Emanuele II 244, 00186 Rome, Italy; matteo.donorio@uniroma1.it
[2] ENEA Fusion and Technology for Nuclear Safety and Security Department, CR Frascati, Via Enrico Fermi 45, 00044 Frascati, Italy
* Correspondence: martina.molinari@uniroma1.it (M.M.); gianfranco.caruso@uniroma1.it (G.C.)

Abstract: Activated Corrosion Product (ACP) formation and deposition pose a critical safety issue for nuclear fusion reactors. The working fluid transports the ACPs towards regions accessible by worker personnel, i.e., the steam generator. The code OSCAR-Fusion has been developed by the CEA (France) to evaluate the ACP generation and transport in closed water-cooled loops for fusion application. This work preliminary assesses the impact of water chemistry on the transport, precipitation, and deposition of corrosion products for the EU-DEMO divertor Plasma Facing Unit Primary Heat Transfer System. Sensitivity analyses and uncertainty quantification are needed due to the multi-physics phenomena involved in ACP formation and transport. The OSCAR-Fusion/RAVEN code coupling developed by the Sapienza University of Rome and ENEA are used. This work presents the perturbation results of different parameters chosen for a closed water-cooled loop considering a continuous scenario of 1888 days. The aim of this work is to preliminarily assess the variation of build-up of ACPs, perturbing the alkalizing agent concentration into the coolant, and the corrosion and release rates of different materials. The assessment of ACP formation deposition and transport is fundamental for source term identification, reduction of radiation exposure assessment, maintenance plan definition, design optimization, and waste management.

Keywords: Activated Corrosion Products; water chemistry; OSCAR; RAVEN; nuclear safety

Citation: Molinari, M.; D'Onorio, M.; Mariano, G.; Terranova, N.; Caruso, G. Water Chemistry Impact on Activated Corrosion Products: An Assessment on Tokamak Reactors. *Energies* **2023**, *16*, 4726. https://doi.org/10.3390/en16124726

Academic Editor: Jerzy A. Szpunar

Received: 11 April 2023
Revised: 30 May 2023
Accepted: 13 June 2023
Published: 15 June 2023

1. Introduction

The ACPs are all the corrosion products formed into a closed coolant loop that are activated under a high neutron flux. In a closed loop of a tokamak reactor, because of coolant transport, the corrosion products are carried from the Out-Flux (OF) region to the In-Flux (IF) region, and vice versa. The corrosion products produced in the OF region will be activated in the IF region, and those produced in the IF region, activated under direct neutron flux, will contaminate the structural material in the OF region. The activation of corrosion products and the contamination of piping surfaces means that there is a production of several radioactive isotopes, such as Co-60 or Mn-54, which have a specific activity of 4.186×10^{13} Bq/g and 2.868×10^{14} Bq/g, respectively.

The ACPs evaluation plays a fundamental role in the safety assessment of fusion reactors [1]. When considering the radioactive contamination of a cooling system of a nuclear plant, the study of ACPs is helpful for the optimization of plant operation, avoiding the damage of the piping materials, as shown in [2] and, at the same time, the reduction of occupational radiation exposure when the source term is considered, as shown in [3]. Moreover, the source term, including ACP, can be mobilized during accident scenarios [4,5].

The ACP generation and transport processes depend on several physical phenomena involving neutronics, thermal–hydraulic, chemical, and geometry aspects. There are several computational tools for the evaluation of ACP generation and transport. One of these is

OSCAR-Fusion [6], developed by the CEA to study the contamination of cooling circuits in the Primary Heat Transfer System (PHTS) of a tokamak reactor.

In each region of the loop, there are two different oxide layers above the base metal: the inner one is adherent to the base metal and is a chromite layer, an oxide mineral composed of chromium oxide with iron oxide (Cr_2FeO_4). The second layer, located above the chromite layer, is a ferrite porous medium layer, an oxide mineral rich in ferric oxide (Fe_2O_3). In the coolant, there are also particles and ions. The fluid transports the particles throughout the loop and comes from the precipitation of ions and erosion of the above-mentioned second oxide layer. The ions, arising from the dissolution of the oxide layer and the base metal, are transported by convection throughout the loop. The sources of these particles and ions or the sink term for the fluid depends on the equilibrium concentration of elements or particles [7].

OSCAR-Fusion allows the study of generation, transport, and activation phenomena to assess the mass associated with an isotope in a given medium at a specific time for each region of the loop. The mass variation is correlated with the various physical mechanisms considered in OSCAR-Fusion and the chemical characteristics of both the materials and the coolant.

Radiolysis is caused by the presence of radiation fields, which results in high oxidizing products [8]. The minimization of the corrosion product built up into a loop can be achieved by optimizing the coolant water chemistry, which can control corrosion phenomena through alkalizing agents and elements able to suppress the oxidizing environment established because of radiolysis.

The alkalizing agents considered for the reducing environment of a Pressurized Water Reactor (PWR), as described in [9], are lithium hydroxide (LiOH), potassium hydroxide (KOH), and ammonia (NH_3) with variable concentrations, depending on the boric acid concentration (H_3BO_3) used for reactivity control. In a nuclear fusion reactor, the presence of H_3BO_3 is not foreseen, but radiolysis is expected because of the high neutron flux. For this reason, an alkalizing agent is expected [10] for pH control and oxidizing environment suppression.

Different experimental analyses have been performed [11] to optimize the water chemistry of tokamak reactors. The impact of water chemistry optimization and practical applications are mainly reactor safety and worker personnel safety. In fact, by assessing the ACP inventory for a cooling loop, occupational radiation exposure can also be evaluated and minimized. Another relevant implication is the optimization of the design when the Safety by Design approach is adopted.

This paper aims to study the impact of water chemistry on ACP generation and transport for a closed loop by perturbing specific parameters that characterize the coolant's chemical composition. This analysis can be performed thanks to the code interface OSCAR-Fusion/RAVEN described in [12] and a Python-based post-processing script. The parametric study is performed considering the EU-DEMO Divertor Plasma Facing Unit PHTS, which verifies the code coupling [10]. The EU-DEMO Divertor has been previously studied to evaluate the mass and activity inventories, as described in [4,13,14].

2. OSCAR-Fusion V1.3

OSCAR-Fusion is a one-dimensional code that focuses on assessing the contamination of a cooling loop, considering different parameters and phenomena. The OSCAR-Fusion code can use physical models implemented to study the mass exchange between the media and the control volumes modeled. Like the previous versions of the code, such as PACTITER, or the ones used in fission (e.g., OSCAR and PACTOLE), described in [7,14–16], the evaluation of the ACPs is based on the mass balance equation, shown in (1).

The OSCAR-Fusion code, in comparison with OSCAR and PACTOLE, is optimized for nuclear fusion operating conditions. Materials such as Cu-based alloys can be modeled, and activation reaction rates for fast neutron flux can be considered [7]. The code has been validated using ~400 EMECC (Ensemble de Mesure et d'Etude de la Contamination

des Circuits) campaigns, through which, as described in [7], the surface activities can be measured and the behavior of the ACPs can be studied.

The variation of a mass M, calculated at each control volume of the isotope *i* in a given medium *j* at time *t*, comes from the mass balance conservation equation [5]:

$$\frac{\partial M_i^j}{\partial t} = \sum Source - \sum Sink + \dot{m}_i - \dot{m}_o \quad (1)$$

where $\dot{m}_i$ and $\dot{m}_o$ are the control volumes inlet and outlet flow rates, respectively.

As described in [7], the media considered are the base metal, the inner oxide layer, the deposit/outer oxide layer, ions, particles, filters, and resins.

Each control volume can describe a closed-loop region, considering given input parameters, such as thermal–hydraulic, neutronic, power distribution, and water chemistry.

The thermal–hydraulic data of the OSCAR-Fusion V1.3 are evaluated by the same formulation of the CATHARE code, which is optionally used to evaluate temperature-dependent variables, such as fluid velocity and density. The PHREEQCEA module evaluates the chemical data.

In OSCAR-Fusion V1.3, the water chemistry characteristics can be evaluated by setting lithium, boron, hydrogen, and oxygen concentration for each period. In OSCAR-Fusion, the lithium concentration corresponds to a lithium hydroxide (LiOH) concentration in water, the boron concentration corresponds to a boric acid (H_3BO_3) concentration in water, and the hydrogen and oxygen concentrations correspond, respectively, to molecular hydrogen (H_2) and molecular oxygen (O_2) in water. It must be highlighted that OSCAR-Fusion V1.3 does not foresee models for radiolysis caused by the radiation field.

In the OSCAR-Fusion code, the default correlations for corrosion rate and release rate are the Moorea laws. The Moorea laws are empirical laws which, for both corrosion rate and release rate, depend on four factors: the standardized coefficient Short-Term Corrosion Rate (STCR) and the Long-Term Corrosion Rate (LTCR), which are functions of the temperature of the fluid; a function related to the pH of the fluid; and an attenuation factor, which, in turn, depends on the ion concentration of a metal species with respect to its equilibrium concentration. Using the default correlations, only a reducing environment can be simulated.

In OSCAR-Fusion V1.3, corrosion and release correlations can also be modeled with user-defined trends, which must follow a power law or logarithmic trend.

3. EU-DEMO Divertor Plasma Facing Unit

The EU-DEMO divertor component is located in the bottom region of the torus. The divertor's role is to reduce the heat flux on the first wall and the helium ashes from the plasma's outer layer, avoiding the build-up and dilution of the plasma ion density and preventing the impurities from entering the plasma core. The DEMO divertor system, as described in [17], is composed of two independent systems, as shown in Figure 1a: the DIVertor CASsette (DIV-CAS) and the DIVertor Plasma Face Unit (DIV-PFU). Both systems are composed of two independent loops, each of them serving 8 of 16 sectors, according to the 2019 design of the Divertor PHTS. A single system of the loop comprises 24 divertor cassettes, three for each sector of the torus.

The components of the EU-DEMO divertor system PHTS are shown in Figure 1b. Each PHTS loop consists of one Heat EXchanger (HEX), one Main Coolant Pump (MCP), one PRessuriZer (PRZ), 8 distributors (DIS), 8 collectors (COL), 24 Hot Feeding Pipes (HFPs), 24 Cold Feeding Pipes (CFPs), one Hot Leg (HL), one Cold Leg (CL), and one Cross-Over Pipe (COV).

Each divertor PFU PHTS cooling loop is operated at a pressure of 3.8 Mpa, with a total mass flow rate of 5319.3 kg/s [17] distributed over the 24 divertor cassettes. The overall PHTS pipe length in the OF region is 2599 m. The cooling water is distributed at 130 °C and is collected at 136 °C. The total PFU PHTS pressure drop is approximately 1960 kPA.

The PFU PHTS comprises AISI316L for the piping system, INCONEL for the HEX for the OF region, and a Cu-based alloy, such as the CuCrZr, for components in the IF region.

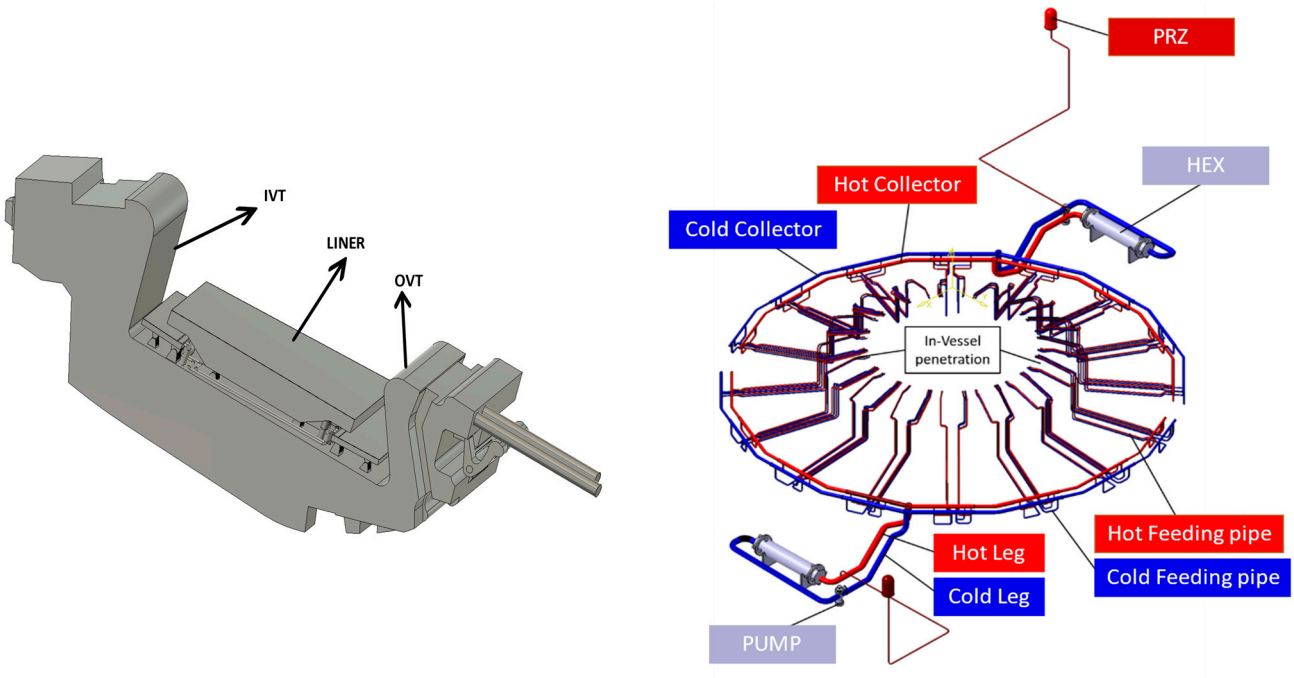

(**a**) (**b**)

Figure 1. (**a**) Divertor assembly; (**b**) Divertor PFU PHTS.

The divertor system PHTS also presents the Chemical Volume Control System (CVCS, labeled as BY in Figure 2), with mechanical filters and ion exchange resins, to maintain the coolant purity and chemical composition.

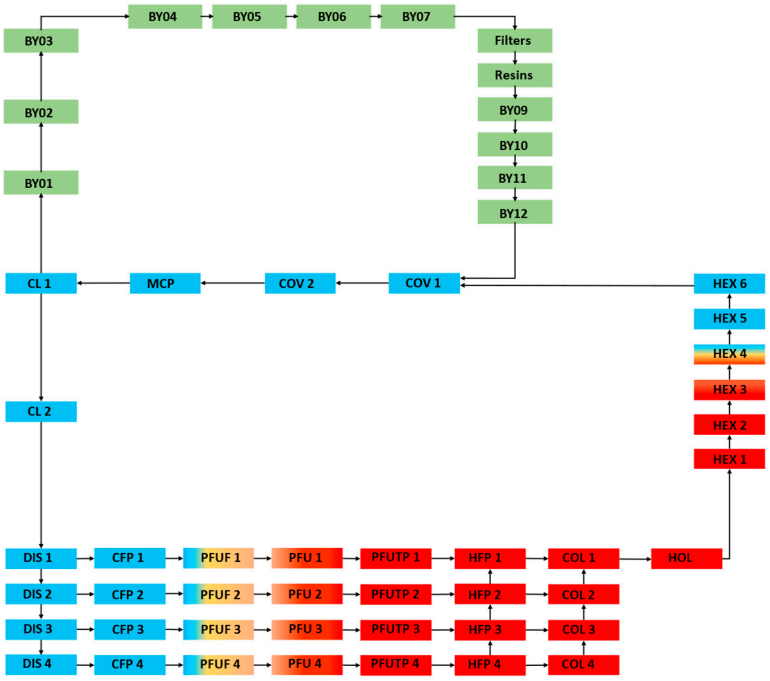

Figure 2. EU-DEMO divertor PFU PHTS OSCAR-Fusion model.

4. OSCAR-Fusion Model of EU-DEMO Divertor PFU

The OSCAR-Fusion model of the divertor PFU PHTS is shown in Figure 2. The model is a simplified closed loop subdivided into 53 regions. Each region has assigned conditions of temperature, pressure, wetted surface, hydraulic diameter, and coolant velocity.

As described in [15], since the CVCS design is not confirmed, some assumptions are made during the modeling phase. The cooling loops are collapsed in half of a single cooling loop using equivalent thermal–hydraulic data. The filters and resin efficiency are set to 99%.

In the OSCAR-Fusion model of the divertor PFU PHTS, four different materials are considered as base metals: Inconel 660, stainless steel SS 316 LN, Metal Cu, and the CuCrZr alloy. For each material, the input chemical parameters are the base metal, the inner/outer oxide layers, and the normalized corrosion coefficients for evaluating the corrosion rate and release rate. The default normalized coefficients are shown in Table 1, where it can be seen that the coefficients are defined before 2 months, which is the STCR, and after 12 months, which is the LTCR. In the interval of 2–12 months, coefficients are correlated between SCTR and LCTR values.

Table 1. Normalized coefficients for corrosion rate and release rate.

Time (Months)	Stainless Steel ($g/s/m^2$)	Copper-Based Alloy ($g/s/m^2$)
$t \leq 2$	1.6×10^{-6}	1.33×10^{-6}
$t > 12$	4.6×10^{-7}	1.33×10^{-6}

The operational scenario adopted for the simulation is a lumped continuous scenario of 1888 days. The temperature and pressure variations inside the loop are imposed as input parameters. The temperature trend in the loop lies in a range of 130 °C–136 °C. The pressure drop is evaluated as 1.960 MPa, as described in 13. The water volume is approximately 114 m^3, and its composition is reported in Table 2. The DEMO water chemistry optimization is preliminarily evaluated and has a pH of approximately 7 at 300 °C [16].

Table 2. Divertor PFU water chemistry parameter.

Chemical Parameter	Concentration
Lithium	0.275 ppm
Boron	0.01 [1] ppm
Hydrogen	25 mL/kg_w
Oxygen	0 ppm

[1] Minimum value allowed in OSCAR-Fusion V1.3.

Using the parameters shown in Table 2 as input, the pH trend in the loop at the initial time of the considered scenario assumes the values depicted in Figure 3a,b. The pH values range in Figure 3a is kept close to neutrality because the pH target is in the range of 7.0 at the operating temperature of the loop.

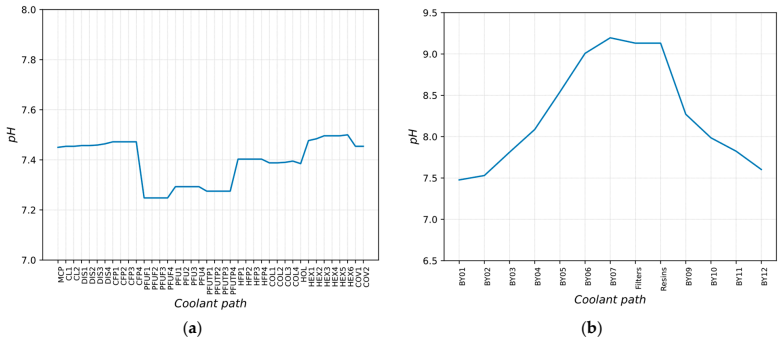

Figure 3. pH trend of the reference case: (**a**) in the loop; (**b**) bypass line.

A difference from neutrality is, therefore, preferable to a slightly alkaline environment because an acid pH can be reached during these operating conditions due to temperature variations and radiolysis reactions.

5. RAVEN/OSCAR-Fusion Analyses

A statistical study with RAVEN/OSCAR-Fusion is performed to assess the impact of water chemistry on ACP generation and transport.

RAVEN is a multi-purpose, probabilistic, and uncertainty framework developed at the Idaho National Laboratory (INL), which can be coupled with any system code [18]. The RAVEN framework is a useful tool through which sensitivity analysis and uncertainty quantification can be performed when coupled with a code. The RAVEN/OSCAR-Fusion interface has already been tested for a preliminary study, as reported in [12]. The RAVEN/OSCAR-Fusion interface uses RAVEN for the sampling phase of the simulation, setting the distribution type and the number of samplings that are to be conducted. When RAVEN completes the sampling phase, the interface starts an OSCAR-Fusion calculation for each sampling conducted by RAVEN.

The OSCAR-Fusion code has its own pre-processor and post-processor for a single input, but there is no available post-processor for multiple simulations; for this reason, Sapienza University developed a Python-based post-processor script to evaluate output files of different simulations in a parallel manner. The Python script elaborates the parameters of interest by creating pivot tables, thanks to which, in this case, the activity related to mass inventory evaluated by the code can be plotted, as discussed in the following paragraphs.

To perform the sensitivity analysis, the parameters to be studied and the perturbation must be identified. This study's parameters are the lithium and hydrogen concentrations in the cooling water. The Figure of Merit (FOM) chosen to evaluate the perturbation's effect is the Mn-54 in the deposit/outer oxide layer medium. The Mn-54 reactions, decay mode, and energy of the γ emitted are summarized in Table 3.

Table 3. Mn-54 reactions and decay characteristics.

Reactions	Father	Decay Mode	Daughter	Energy (keV)	$T_{\frac{1}{2}}$ (d)
Mn-53 (n, γ) Mn-54 Mn-55 (n, 2n) Mn-54 Fe-54 (n, p) Mn-54 Fe-54 (n, np) Mn-53 (n, γ) Mn-54	Mn-54	Electronic capture	Cr-54	834.855	312.19

For both case studies, 100 runs are performed. The total number of runs is evaluated using Wilk's formula, as described in [19,20]. Pearson's and Spearman's coefficients are used to quantify the correlation between the variables [20,21].

The reaction rates considered in the reference case are summarized in Table 4.

Table 4. Nuclear reaction rates.

Reaction	Reaction Rate (1/s)
Mn-53 (n, γ) Mn-54	7.451×10^{-10}
Mn-55 (n, 2n) Mn-54	1.253×10^{-11}
Fe-54 (n, p) Mn-54	8.946×10^{-12}
Fe-54 (n, np) Mn-53	1.036×10^{-11}

6. Results for Case Study 1: Lithium Concentration

The lithium concentration is perturbed starting from the divertor system's water chemistry parameters, as summarized in Table 2.

The lithium concentration represents the only alkalizing agent which can be simulated in OSCAR-Fusion V1.3. The perturbation of LiOH concentration in water means a variation in pH and, therefore, the increase or reduction in the corrosion rate. The perturbation of lithium concentration is reported in Table 5.

Table 5. Case Study 1—sampling.

Lithium Concentration (Uniform Distribution) (ppm)	
Lower Bound (LB)	Upper Bound (UB)
0.0	1.5 [2]

[2] Maximum value allowed in OSCAR-Fusion V1.3.

The 100 runs completed by the code are statistically analyzed, showing that the lithium concentration perturbation leads to the range of values depicted in Figure 4a,b. It is possible to notice a trend in which the pH increases when the concentration of LiOH increases.

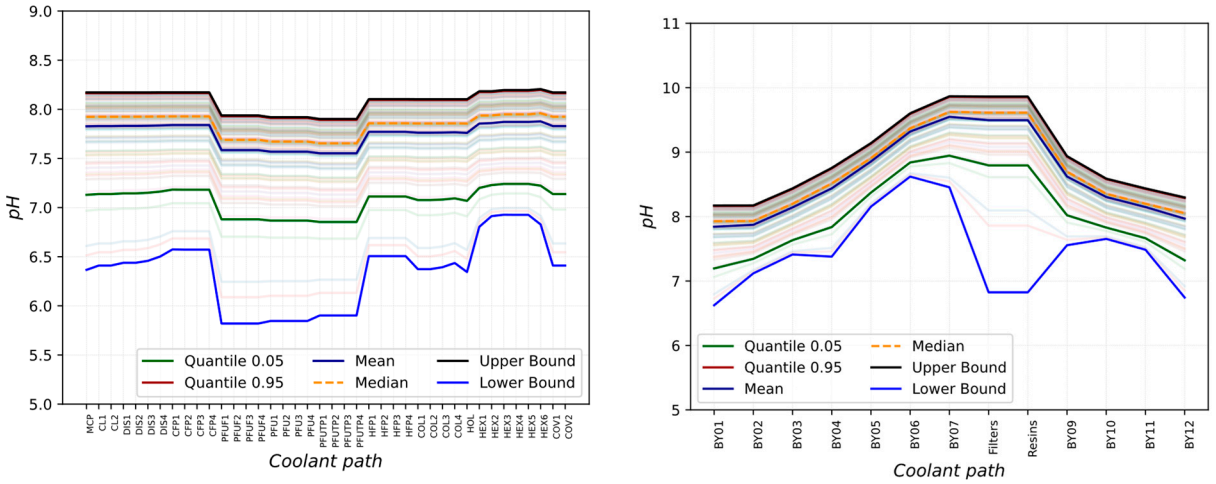

Figure 4. pH trend after Li concentration perturbation: (**a**) in the loop; (**b**) bypass line.

Because Mn-54 can also be obtained from Fe-54, both the Mn and Fe corrosion rates must be considered. During the entire simulation, there is variation in the corrosion rates of both Mn and Fe in the deposit/outer oxide layer medium caused by the pH variation. The deposit/outer oxide layer formation mechanism increases by varying the corrosion rate. Figure 5a shows the main statistical parameters evaluated for the FOM.

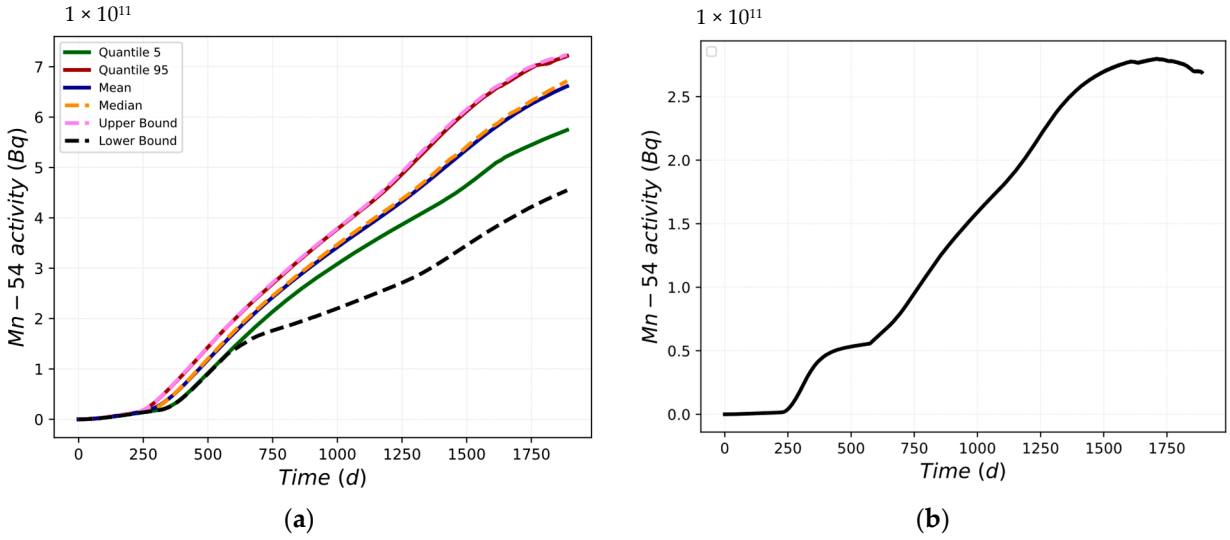

Figure 5. (**a**) Mn-54 activity in the deposit/outer oxide layer; (**b**) Mn-54 activity difference between UB and LB.

As can be seen in Figure 5b, the difference between the UB trend and the LB trend is time-dependent. Figure 5b highlights a maximum difference of 2.79 $\times$ 10^{11} Bq and a difference at the end of the scenario of 2.69 $\times$ 10^{11} Bq.

The analyzed data increasingly deviate from the trend of the mean value. Figure 6a shows the mean value trend, while Figure 6b depicts the standard deviation trend of the Mn-54 activity into the loop. The standard deviation trend is also predictable from Figure 5a. The variability of the data increases at approximately 600 days and tends to decrease at approximately 1500 days. This reduction is also confirmed by the variation in the slope of the first derivative in the same moments as in Figure 5b.

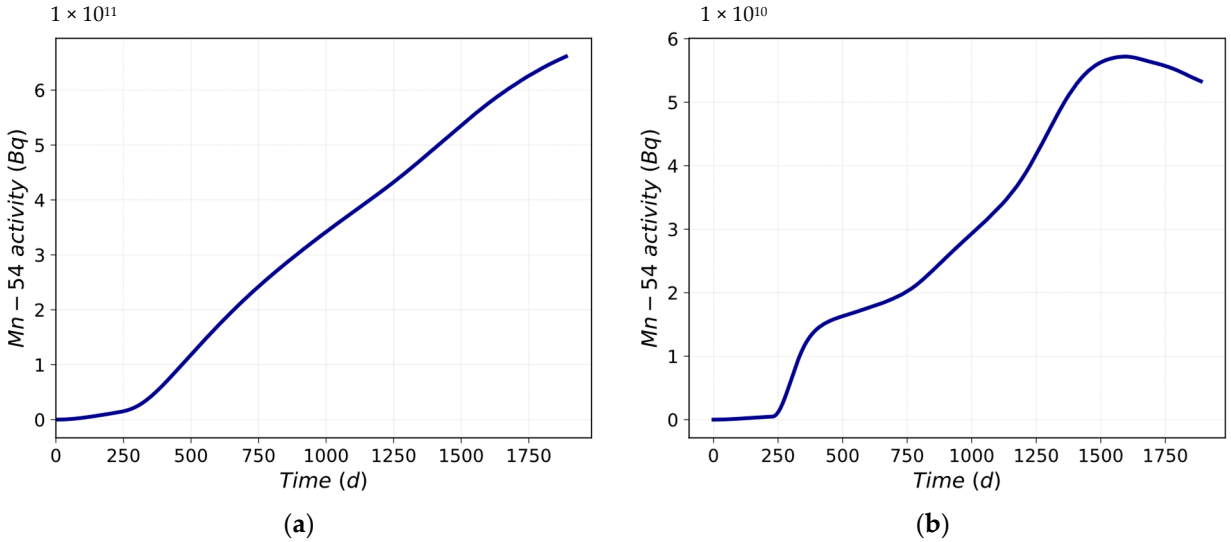

Figure 6. Mn-54 activity: (**a**) mean value trend; (**b**) standard deviation trend.

In Figure 7, the Probability Density Function (PDF) evaluated at the end of the scenario is shown. A platykurtic and non-symmetric distribution, centered in 6.61 $\times$ 10^{11} Bq, is obtained. The kurtosis and skewness values reported in Table 6 confirm the PDF characteristics.

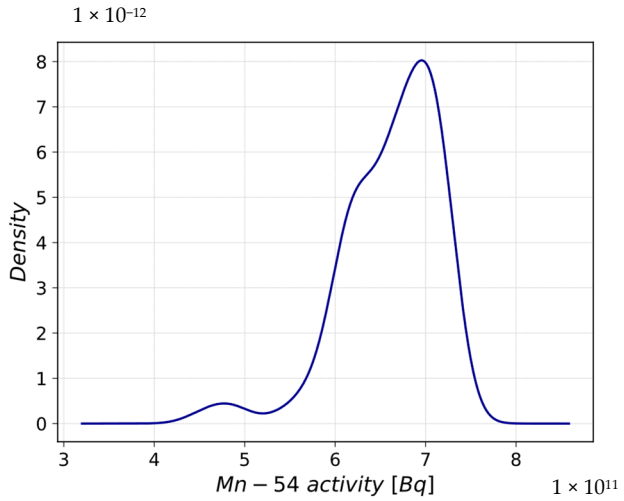

Figure 7. Probability Density Function of Mn-54 activity after LiOH concentration perturbation.

Table 6. PDF description factors for LiOH concentration perturbation.

Kurtosis	−1.38	k < 0: the PDF is platykurtic
Skewness	0.54	s > 0: data are skewed to the righ

Figure 8a,b highlight that by perturbing the LiOH concentration, there is a variation in the Mn54 activity in the deposit medium. After 3 days from the beginning of the scenario, the correlation between the perturbed parameter and the FOM is at the highest value, as shown in Figure 9a,b by Pearson's and Spearman's correlation coefficients. Pearson's correlation is a measure of linear correlation between two sets of data [22], whereas Spearman's correlation is the measure of the monotonic relation between the ranked values of two sets of data [21]. This means that the correlation between the LiOH concentration perturbation and Mn-54 activity in the deposit/outer oxide layer is neither linear nor monotonic, and there is a weak correlation between the LiOH concentration and the FOM.

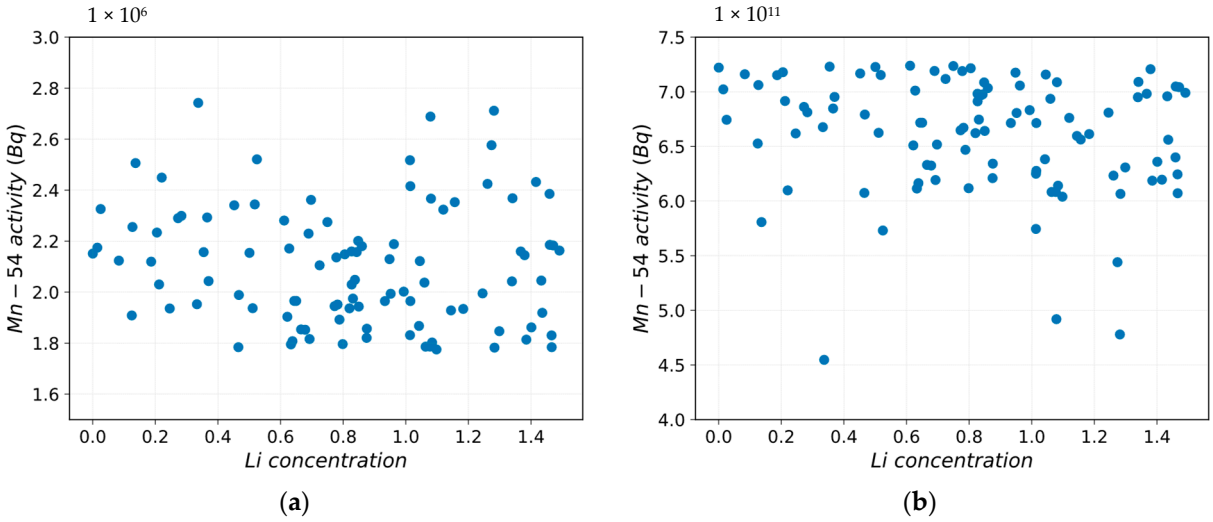

(**a**) (**b**)

Figure 8. Mn-54 activity vs. Li concentration: (**a**) after 3 days; (**b**) after 1888 days.

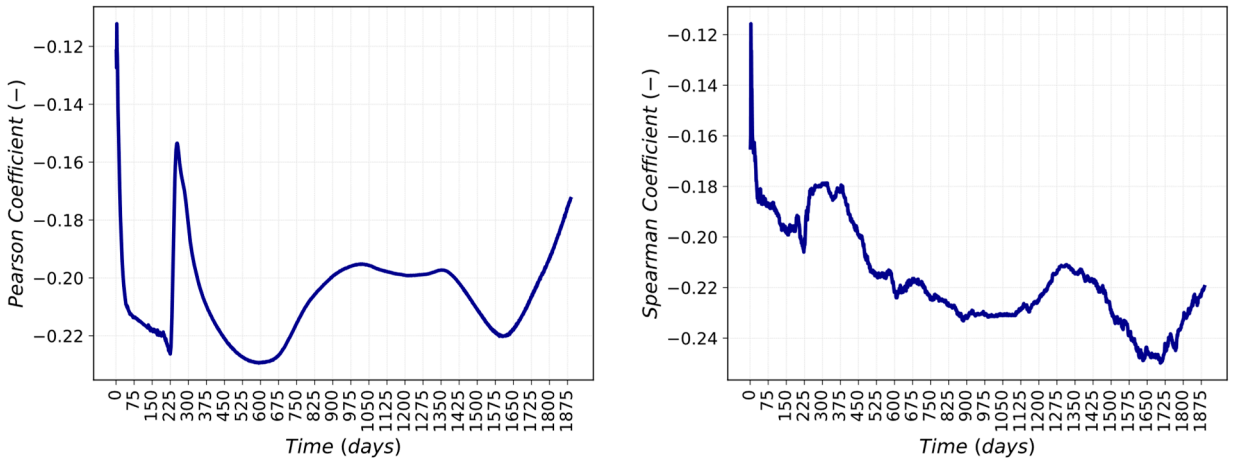

(**a**) (**b**)

Figure 9. Correlations between Mn-54 activity in deposit and Li concentration: (**a**) Pearson; (**b**) Spearman.

7. Results for Case Study 2: Corrosion Rates

When editing the laws of corrosion and release models, the OSCAR-Fusion code requires several parameters, some of which are the standardized coefficient for corrosion rates for the copper-based alloy and stainless steel. The default parameters are shown in Table 2.

In order to evaluate the CP formation and activation, the standardized coefficients for corrosion rates are taken into account. The perturbation of the standardized coefficient for corrosion rates is reported in Table 7. For the Cu-based alloy, the UB and LB are chosen by

considering the oxidizing condition described in [23] at 130 °C and a fluid velocity of 13 $\frac{m}{s}$. The UB and LB values are selected in order to have a non-negligible perturbation on the corrosion rate and release rate of the materials considered into the loop.

Table 7. Case Study 2—sampling.

Standardised Coefficients for Corrosion Rates (Uniform Distribution) (g/m^2/s)		
Coefficient	**UB**	**LB**
Copper-based alloy	1.22×10^{-5}	7.67×10^{-6}
Stainless Steel STCR	5×10^{-6}	5×10^{-7}
Stainless Steel LTCR	1×10^{-6}	1×1^{-7}

The 100 runs completed by the code are statistically analyzed and, as in the previous case, Mn and Fe corrosion rates are considered. During the entire simulation, there is a variation in the corrosion rate in the deposit/outer oxide layer caused by the induced perturbation. The deposit/outer oxide layer formation mechanism increases by varying the corrosion rate.

Figure 10a shows the main statistical parameters evaluated for the selected FOM, the Mn-54 activity in the deposit/outer oxide layer, while Figure 10b shows the difference in the activity of UB and LB. Maximum differences of 7.45×10^9 Bq and of 7.26×10^9 Bq at the end of the considered scenario are obtained.

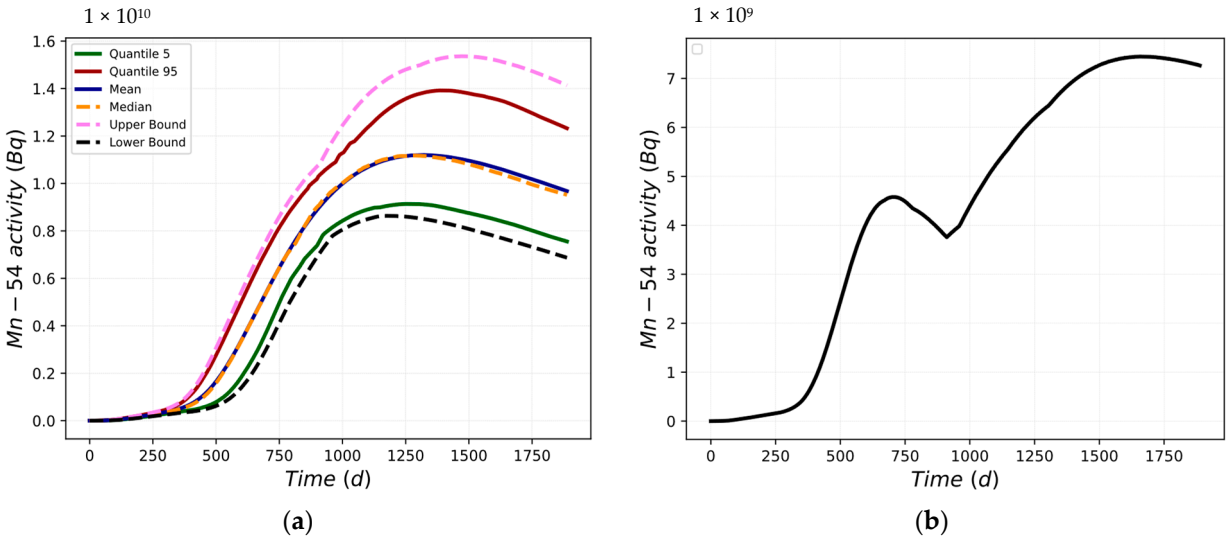

(**a**) (**b**)

Figure 10. Mn-54 activity: (**a**) statistical parameters; (**b**) difference between UB and LB.

In Figure 11a, the mean value trend is shown, while Figure 11b depicts the standard deviation trend of the Mn-54 activity into the loop. It can be seen that the analyzed data deviation increases with time. The standard deviation trend is predictable, taking into account the statistical parameters. In Figure 10a, at approximately 400 days, there is an increase in the variability of the data up to the first point of maximum at approximately 700 days. After 700 days, there is a decrease until the 900th day. After that, the standard deviation increases again until the second maximum point is reached, at approximately 1550 days. After 1550 days, the variability of the data tends to reduce.

In Figure 12, the PDF evaluated at the end of the scenario is reported, showing a platykurtic and quasi-symmetric distribution centered at 9.67×10^9, which is the mean value. The PDF characteristics are confirmed by the kurtosis and skewness values in Table 8.

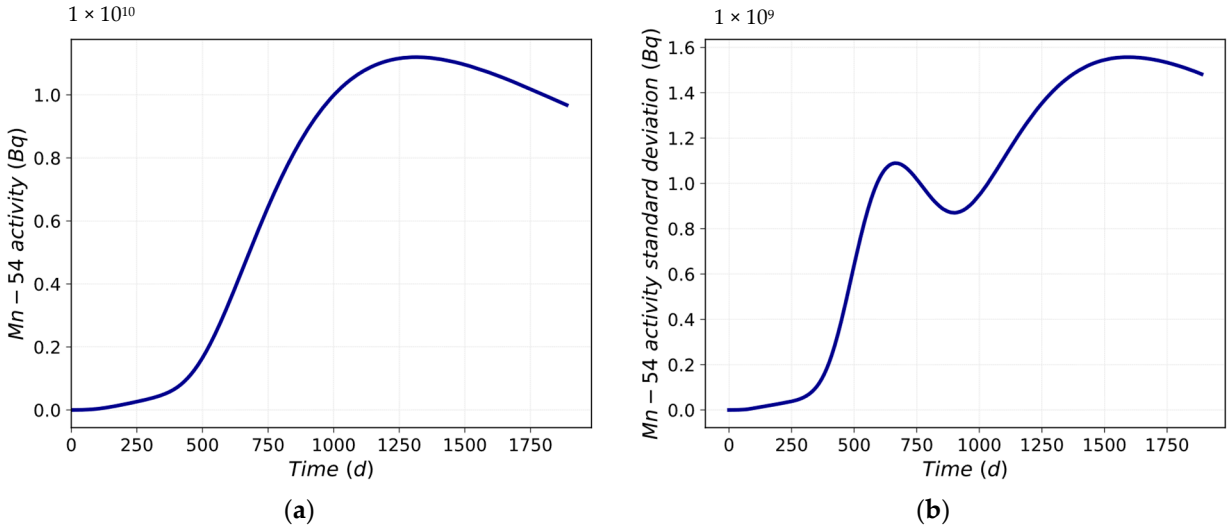

Figure 11. Mn-54 activity trend: (**a**) mean value; (**b**) standard deviation.

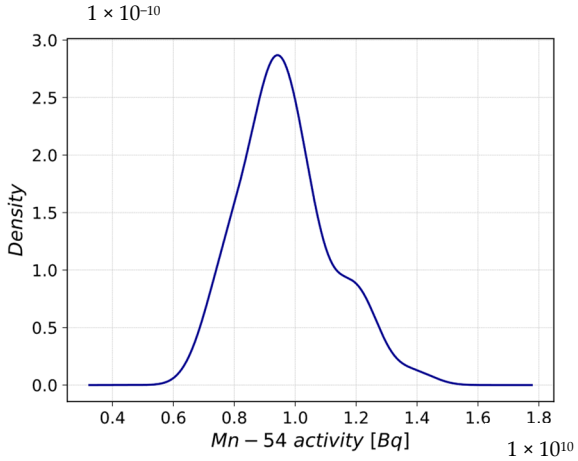

Figure 12. Probability Density Function of Mn-54 activity after corrosion rate perturbation.

Table 8. PDF description factors for corrosion rate perturbation.

Kurtosis	−1.441	k < 0: the PDF is platykurtic
Skewness	0.02	s > 0: data are skewed to the right

Figures 13 and 14a,b highlight that there is a variation in the Mn-54 activity in the deposit medium by perturbing the standardized coefficients for corrosion rates.

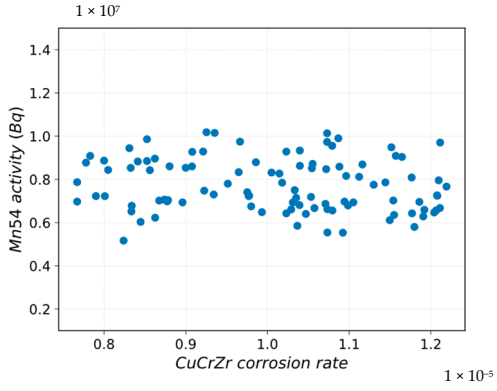

Figure 13. Mn-54 activity vs. CuCrZr corrosion rate sampling.

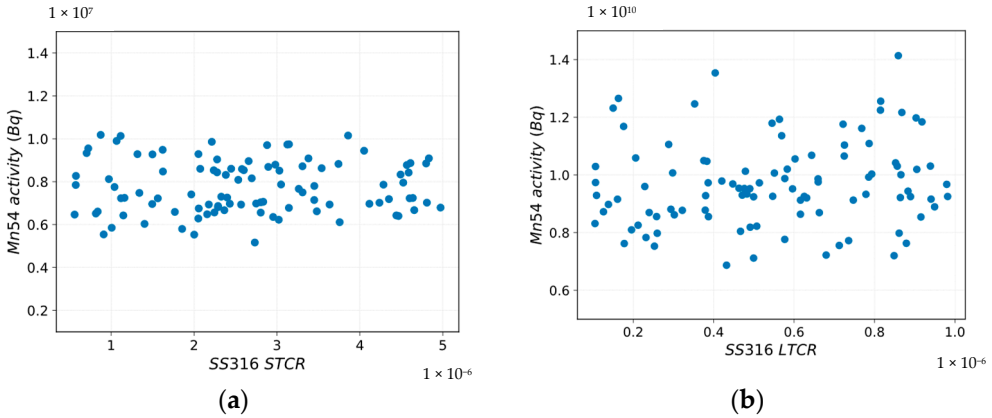

(**a**) (**b**)

Figure 14. Mn-54 activity vs. SS316 sampling: (**a**) STCR; (**b**) LTCR.

Pearson's and Spearman's partial correlations coefficients are shown in Figures 15 and 16a,b. The correlation between the normalized coefficients of the Cu-based alloy and Mn-54 activity in the deposit/outer oxide layer is linear and monotonic from the beginning of the simulation until 800 days and from 1000 days until the end of the scenario.

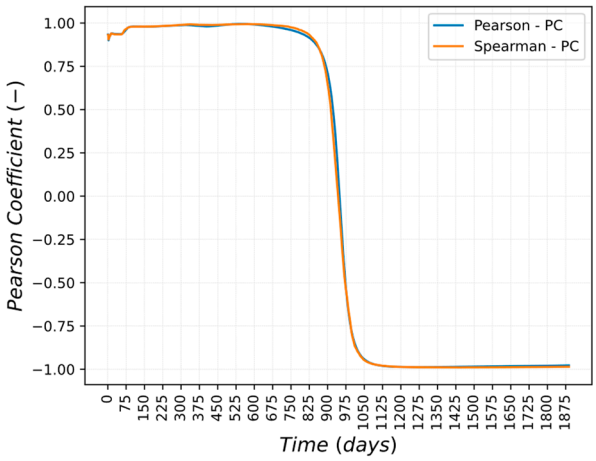

Figure 15. Pearson and Spearman Partial Correlation trend for CuCrZr perturbation.

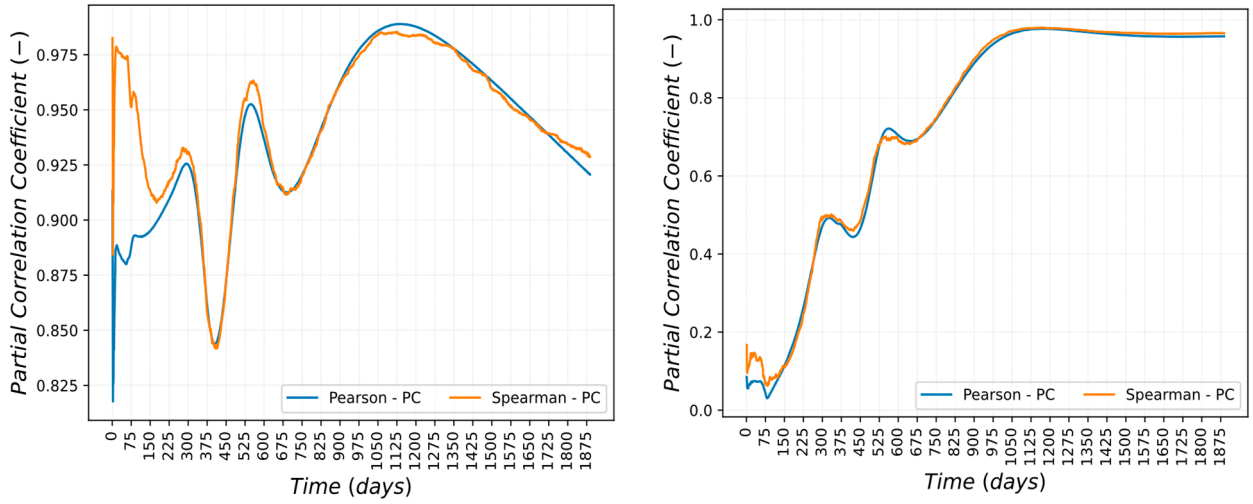

(**a**) (**b**)

Figure 16. Pearson and Spearman Partial Correlation trend: (**a**) STCR perturbation; (**b**) LTCR perturbation.

The correlation between the STCR and the Mn-54 activity in the deposit/outer oxide layer is strong for the entire scenario considered. Therefore, it can be concluded that the correlation is both linear and monotonic.

The correlation between the LTCR and the Mn-54 activity in the deposit/outer oxide layer is linear and monotonic from approximately 900 days until the end of the scenario considered.

8. Conclusions and Future Work

The impact of water chemistry on ACPs has been studied through the perturbation of chemical parameters, such as the LiOH concentration and the corrosion rates of different materials. The model used in OSCAR-Fusion V1.3 was a simplified but representative reproduction of the EU-DEMO PFU.

Two different case studies have been analyzed. Case Study 1 demonstrated that, due to the LiOH concentration perturbation, there was an impact on Mn-54 activity in the deposit/outer oxide layer of the whole loop. Case Study 2 showed how the perturbation of normalized corrosion coefficients could significantly impact the Mn-54 activity in the deposit/outer oxide layer.

The perturbation of normalized corrosion coefficients led to a variation in the cooling circuit's corrosion rate and release rate. It must be noted that the perturbation on LiOH led to a pH variation in the cooling circuit. The pH is a parameter on which the corrosion rate depends when the Moorea law is set as the corrosion release law. The corrosion rate formulation depends on four different parameters: temperature, pH, equilibrium concentration, and normalized corrosion coefficients for the STCR and LTCR.

For Case Study 1, the statistical analysis has shown that the correlation between the perturbed parameter and the Mn-54 activity in the loop's deposit/outer oxide layer was not linear or monotonic. For Case Study 2, the statistical analysis has shown that the correlation between the perturbed parameters and the Mn-54 activity in the deposit/outer oxide layer in the loop was linear and monotonic in most of the considered scenarios.

These analyses, despite being preliminary, suggested that the perturbation of the water chemistry composition had an impact on the ACPs, but it was not always observable with the Pearson and Spearman correlations or the Pearson and Spearman partial correlations.

Optimizing the water chemistry led to a reduction of corrosion products into a coolant loop; this signified a reduction of the build-up of ACPs and, thus, the specific activity of one or more components during the planned maintenance or at the end of their life cycle. Consequently, with water chemistry control, it was possible to reduce occupational radiation exposure during both the maintenance and the decommissioning phases.

As previously stated, OSCAR-Fusion V1.3 does not foresee physical models for radiolysis. As described in [24], there was a more oxidizing environment due to radiolysis relative to the one modeled by OSCAR-Fusion V1.3; this was due to the presence of free radicals and molecules that were more oxidizing than O_2, such as hydrogen peroxide or hydroperoxide.

Considering the preliminary nature of this water chemistry analysis, more detailed studies will be performed to analyze the impact of oxygen perturbation and other alkalizing agents with a new version of the computer code, OSCAR-Fusion V1.4, and the subsequent versions.

Author Contributions: Conceptualization, M.M., M.D. and G.C.; methodology, M.M., M.D., N.T. and G.C.; software M.D., G.M. and N.T., writing—original draft preparation M.M., M.D., N.T. and G.C.; writing, review and editing M.M., M.D., G.M., N.T. and G.C. All authors have read and agreed to the published version of the manuscript.

Funding: This work was carried out within the framework of the EUROfusion Consortium, funded by the European Union via the Euratom Research and Training Program (Grant Agreement No 101052200—EUROfusion). The views and opinions expressed are, however, those of the author(s) only and do not necessarily reflect those of the European Union or the European Commission. Neither the European Union nor the European Commission can be held responsible for them.

Data Availability Statement: Data are available only for institutions involved in the EUROfusion project. For that organization the data presented in this study are available on request from the corresponding author.

Conflicts of Interest: The authors declare no conflict of interest. The funders had no role in the design of the study; in the collection, analyses or interpretation of data, in the writing of the manuscript, or in decision to publish the results.

List of Abbreviations

ACP	Activated Corrosion Products
CB	Cassette body
CFP	Cold feeding pipes
CL	Cold leg
COV	Cross-over pipe
CVCS	Chemical volume control system
FOM	Figure of merit
HEX	Heat exchanger
HFP	Hot feeding pipe
HL	Hot leg
IF	In-flux
INL	Idaho National Laboratory
IVT	Inner vertical target
LB	Lower bound
LTCR	Long-term corrosion rate
MCP	Main coolant pump
OF	Out-flux
OSCAR	Tool for simulating contamination in reactors
OVT	Outer vertical target
PFU	Plasma facing units
PHTS	Primary heat transfer system
PRZ	Pressurizer
PWR	Pressurized water reactor
RP	Reflector plates
SL	Shielding liner
STCR	Short-term corrosion rate
UB	Upper bound

References

1. Caruso, G.; Ciattaglia, S.; Colling, B.; Di Pace, L.; Dongiovanni, D.N.; D'Onorio, M.; Garcia, M.; Jin, X.Z.; Johnston, J.; Leichtle, D.; et al. DEMO—The main achievements of the Pre-Concept phase of the safety and environmental work package and the development of the GSSR. *Fus. Eng. Des.* **2022**, *176*, 113025. [CrossRef]
2. Mustafa Azeem, M.; Zubair, M.; Ado, M.; Adb El Gawad, K.; Adam Ibrahim, S.; Mehdi, G. Radiation damage effects in oxide dispersion strengthened steel alloys. In Proceedings of the 27th International Conference on Nuclear Engineering, Tsukuba, Japan, 19–24 May 2019.
3. Zubair, M.; Ahmed, E.; Hartano, D. Estimation of public exposure during normal operation of unit-1 Barakah Nuclear Power Plant using GALE and HOTSPOT. *S. Afr. J. Chem. Eng.* **2022**, *41*, 235–243. [CrossRef]
4. Dongiovanni, D.N.; D'Onorio, M.; Caruso, G.; Pinna, T.; Porfiri, M.T. DEMO Divertor Cassette and Plasma facing Unit in Vessel Loss-of-Coolant Accident. *Energies* **2022**, *15*, 8879. [CrossRef]
5. D'Onorio, M.; Glingler, T.; Porfiri, M.T.; Dorngiovanni, D.N.; Ciattaglia, S.; Gliss, C.; Elbez-Uzan, J.; Cortes, P.; Caruso, G. Development of a Thermal-Hydraulic Model for the EU-DEMO Tokamak Building and LOCA Simulation. *Energies* **2023**, *16*, 1149. [CrossRef]
6. Rafique, M.; Mirza, N.M.; Mirza, S.M.; Iqbal, M.J. Review of computer codes for modelling corrosion product transport and activity build-up in light water reactors. *Nukleonika* **2010**, *55*, 263–269.
7. Daquait, F.; Génin, J.B.; Brissonneau, L. Modelling of the contamination transfer in nuclear reactors: The OSCAR code—Applications to SFR and ITER. In Proceedings of the 1st IAEA Workshop on Challenges for Coolants in Fast Neutron Spectrum Systems, Vienna, Austria, 5–7 July 2017.
8. Macdonald, D.D.; Engelhardt, G.R.; Petrov, A. A critical review of radiolysis issues in water-cooled fission and fusion reactors: Part I, assessment of radiolysis models. *Corros. Mater. Degrad.* **2022**, *3*, 470–535. [CrossRef]

9. International Atomic Energy Agency. *Reactor Water Chemistry Relevant to Coolant-Cladding Interaction*; IAEA: Vienna, Austria, 1987.
10. Harrington, C.; Oron-Carl, M. *Corrosion and Chemistry Control for the WCLL System with Investigation of Corrosion Mechanisms of Eurofer in Aqueous Solutions*; Report IDM, EDFA_D_2NTPBQ; EUROfusion: Garching, Germany, 2021.
11. Lo Piccolo, E.; Torella, R.; Terranova, N.; Di Pace, L.; Gasparrini, C.; Dalla Palma, M. Preliminary assessment of cooling water chemistry for fusion power plants. *Corros. Mater. Degrad.* **2021**, *2*, 512–530. [CrossRef]
12. D'Onorio, M.; Molinari, M.; Mariano, G.; Terranova, N. RAVEN/OSCAR-Fusion coupling for activated corrosion products assessments, sensitivity and uncertainty quantification. *IEEE Trans. Plasma Sci.* **2022**, *50*, 4527–4532. [CrossRef]
13. CEA. *La Corrosion et L'altération des Matèriaux du Nuclèaire*; CEA Saclay et Group Moniteur (Éditions du Moniteur): Paris, France, 2010.
14. Di Pace, L. *Activated Corrosion Products Assessment in Fusion Reactors*; ENEA CR: Frascati, Italy, 2019.
15. Terranova, N. *Activation Corrosion Products (ACP) Assessment*; Report IDM, EDFA_D_XYZ123; EUROfusion: Garching, Germany, 2020.
16. Terranova, N. *ACPs Assessment for DEMO Divertor Cooling Loop*; Report IDM, EDFA_D_2P9QUG; EUROfusion: Garching, Germany, 2022.
17. Narcisi, V.; Frullini, M.; Giannetti, F. *WCLL DIV-PFU PHTS DDD (Direct Coupling Option with Small ESS)*; Report IDM, EDFA_D_2ND5SH; EUROfusion: Garching, Germany, 2020.
18. Rabiti, C.; Alfonsi, A.; Cogliati, J.; Mandelli, D.; Kinoshita, R.; Sen, S.; Wang, C.; Talbot, P.W.; Maljovec, D.P.; Chen, J. *RAVEN User Manual*; Idaho National Laboratory: Idaho Falls, ID, USA, 2017.
19. Wilks, S.S. Determination of sample size for setting tolerance limits. *Ann. Math. Stat.* **1941**, *12*, 91–96. [CrossRef]
20. Wilks, S.S. Statistical prediction with special reference to the problem of tolerance limits. *Ann. Math. Stat.* **1942**, *13*, 400–409. [CrossRef]
21. Dodge, Y. Spearman Rank Correlation Coefficient. In *The Concise Encyclopedia of Statistics*, 1st ed.; Springer: New York, NY, USA, 2008; pp. 502–505. [CrossRef]
22. Kirch, W. Pearson's Correlation Coefficient. In *The Encyclopedia of Public Health*; Springer: Dordrecht, The Netherlands, 2008; pp. 1090–1091. [CrossRef]
23. Obitz, C.; Öijerholm, J.; Wikman, S.; Bratu, E. Erosion corrosion of CuCrZr specimens exposed for simulated ITER operational conditions. *Nucl. Mater.* **2016**, *9*, 261–266. [CrossRef]
24. Harrington, C.; Baron-Wiechec, A.; Burrows, R.; Holmes, R.; Clark, R.; Walters, S.; Martin, T.L.; Springell, R.; Öijerholm, J.; Becker, R.; et al. Chemistry and corrosion research and development for the water cooling circuits of European DEMO. *Fus. Eng. Des.* **2019**, *146*, 478–481. [CrossRef]